Molecular Pharmacology Fast Forward. Published on December 9, 2015 as DOI: 10.1124/mol.115.100149
This article has not been copyedited and formatted. The final version may differ from this version.

TITLE PAGE

Structural insights into the pharmacophore of vinca domain inhibitors of microtubules

Yuxi Wang, Frederick W. Benz, Yangping Wu, Qisheng Wang, Yunfeng Chen, Xiangzheng Chen, Huiyan Li, Yonghui Zhang, Rundong Zhang, Jinliang Yang

State Key Laboratory of Biotherapy and Cancer Center, West China Hospital, Sichuan University, and Collaborative Innovation Center for Biotherapy, Chengdu, 610041, P.R. China(Y.W.,Y.W.,Y.C.,X.C.,H.L.,R.Z.,J.Y.);

Department of Pharmacology and Toxicology, University of Louisville School of Medicine, Health Sciences Center, Louisville, KY 40292(F.W.B.);

Shanghai Synchrotron Radiation Facility and Shanghai Institute of Sciences, 239 Zheng Heng Road, Pudong New District, Shanghai, 201204 P.R. China (Q.W.);

Pharmacology & Pharmaceutical Sciences School of Medicine, Tsinghua University and Collaborative Innovation Center for Biotherapy, Beijing, 100084, P. R. China (Y.Z.)

Molecular Pharmacology Fast Forward. Published on December 9, 2015 as DOI: 10.1124/mol.115.100149
This article has not been copyedited and formatted. The final version may differ from this version.

Running title:

Pharmacophore of vinca domain inhibitors of microtubules

Corresponding authors:

Jinliang Yang jinliangyang@scu.edu.cn and Rundong Zhang rundongzhang@scu.edu.cn

3-17 Renmin South Road, State Key Laboratory of Biotherapy and Cancer Center, West China Hospital, Sichuan University, and Collaborative Innovation Center for Biotherapy, Chengdu, 610041, P.R. China

Phone: +86-28-85502796. Fax: +86-28-85502796.

The number of text pages, 27

The number of tables, 1

The number of figures, 6

The number of references, 28

The words in the abstract, 245 words

The words in the introduction, 749 words

The words in the discussion, 985 words

ABBREVIATIONS: ADCs, antibody-drug conjugates; MTAs, microtubule-targeting agents; DMSO, dimethylsulfoxide; RB3-SLD, stathmin-like domain of RB3; TTL, tubulin tyrosine ligase; T2-R-TTL, consisting of α/β-tubulin, the stathmin-like protein RB3 and tubulin tyrosine ligase; AMPPCP, β,γ-Methyleneadenosine 5′-triphosphate disodium salt; DTT, Dithiothreitol; EGTA, Ethylene glycol-bis(2-aminoethylether)-N,N,N,N-tetraacetic acid; GTP, Guanosine 5′-triphosphate sodium salt hydrate.

Molecular Pharmacology Fast Forward. Published on December 9, 2015 as DOI: 10.1124/mol.115.100149
This article has not been copyedited and formatted. The final version may differ from this version.

ABSTRACT

Antibody-drug conjugates (ADCs) have achieved great success in cancer therapy in recent years. Some peptidyl microtubule inhibitors consisting of natural and unnatural amino acids, such as MMAE and MMAF, are extremely cytotoxic and have been used as a payload in ADCs. However, their precise molecular interaction with tubulin and microtubules remains unclear. We determined the crystal structures of tubulin in complex with three ultra-potent peptidyl microtubule inhibitors, MMAE, HTI-286 and tubulysin M at 2.5Å. Our data showed that the three peptides bound to the vinca domain and shared a common and key pharmacophore containing two consecutive hydrophobic groups (Val, Ile-like side chain). These groups protruded in opposite directions into hydrophobic pockets on the tubulin β and α subunits. Nitrogen and oxygen atoms from the same backbone formed hydrogen bonds with Asn329 from the α subunit and Asp179 from the β subunit in a direction normal to the surface formed by the above hydrophobic groups. In addition, our crystal structure data indicated that tubulysin M bound to the β subunit alone providing a structural explanation for its higher affinity. We also compared the conformations of two representative structurally different vinca domain compounds ustiloxin D and vinblastine with those of the above peptidyl ligands, and found that they shared a similar pharmacophore. Our findings lay a foundation for the rational design of novel vinca domain ligands and may facilitate the development of microtubule inhibitors with high specificity, affinity and efficiency as payloads for ADCs in cancer therapy.

Molecular Pharmacology Fast Forward. Published on December 9, 2015 as DOI: 10.1124/mol.115.100149
This article has not been copyedited and formatted. The final version may differ from this version.

Introduction

Microtubules, highly dynamic structures of the cytoskeleton composed of tubulin, play crucial roles in cell mitosis, growth and movement (Akhmanova and Steinmetz, 2008; Etienne-Manneville and Hall, 2002). The biological functions of microtubules are mainly regulated by polymerization and depolymerization of the α- and β-tubulin heterodimers (Etienne-Manneville, 2010). Microtubules and tubulin have been important cancer chemotherapy targets for decades, and microtubule-targeting agents (MTAs) can efficiently result in mitotic arrest and cell death (Cragg and Newman, 2004; Dumontet and Jordan, 2010). To date, several dozen MTAs have been discovered and developed, such as paclitaxel (Komlodi-Pasztor et al., 2012), vinblastine (Carlson and Ocean, 2011) and epothilone (Roque et al., 2013). Among them, paclitaxel and vinblastine represent a very successful class of anticancer drugs widely used clinically for the treatment of leukemias, lymphomas, and some solid malignancies (Muldoon et al., 2007; Risinger et al., 2009).

MTAs can bind to tubulin directly causing conformational changes thus interfering with microtubule structure and dynamics. MTAs are divided into two general categories: microtubule stabilizing and destabilizing agents (Hartley et al., 2012). Microtubule stabilizing agents, represented by taxol-like compounds, bind to the lateral side of tubulin, stabilizing the M-loop of β-tubulin, which establishes the lateral contacts of tubulin in microtubules(Prota et al., 2013a). Microtubule destabilizing agents bind to the longitudinal interface between the α/β tubulin subunits, causing conformational shifts of consecutive α, β-tubulin heterodimers from a straight to a curved form, facilitating microtubule disassembly(Gigant et al., 2005; Ravelli et al., 2004). Based upon the specific interface to which they bind, microtubule destabilizing agents can be further subdivided into a colchicine-like group that binds to the α/β interface within one tubulin heterodimer (intra-dimer), termed the colchicine site, or into a

Molecular Pharmacology Fast Forward. Published on December 9, 2015 as DOI: 10.1124/mol.115.100149
This article has not been copyedited and formatted. The final version may differ from this version.

vinblastine-like group, that binds to the α/β interface between two tubulin heterodimers (inter-dimer), named the vinca domain. Colchicine site ligands bind deeply into the small hydrophobic pocket formed primarily by β-tubulin and are, in general, structurally small making further modifications of this type of ligand more problematic. In contrast, vinca domain ligands bind to the interface formed by two tubulin heterodimers and are, in general, structurally larger. This feature not only provides for more structural diversity, but also the opportunity for higher affinity for tubulin and greater cytotoxicity. Some MTAs, such as HTI-286, MMAE and tubulysin M (Fig. 1), are extremely cytotoxic with in vitro IC50 values in the nmol to pmol range (typically 100-1,000-fold lower than vinblastine and taxol). When used alone these agents are unsuitable clinically because of their narrow therapeutic window. However, they have recently been used successfully in clinical applications as payloads on antibody-drug conjugates (ADCs) to increase their target specificity. For example, Adcetris, an ADC with MMAE as the payload, was the first FDA-approved ADC for Hodgkin disease in 2011(Klute et al., 2014).

Structural studies of the binding of vinca domain ligands with tubulin have facilitated our understanding of their mechanism of interaction and have provided the basis for rational drug design. Efforts in this direction began in 2005 when the crystal structure of vinblastine bound to tubulin was determined at 4.1Å. Subsequently, the conformation of several additional vinca domain ligands bound to tubulin have been studied, such as soblidotin (Cormier et al., 2008) and ustiloxin D (Ranaivoson et al., 2012).With the exception of ustiloxin D at 2.7Å resolution, all the others were determined at intermediate resolutions (>3.5Å), which cannot provide sufficient structural detail critical for rational drug design. MMAE, the payload of Adcetris, HTI-286 (Poruchynsky et al., 2004) and tubulysins (Cohen et al., 2014) are vinca domain ligands of linear tri- or tetrapeptides composed of diverse unnatural amino acids with ultra-potent cytotoxicity. The details of how these agents bind to

Molecular Pharmacology Fast Forward. Published on December 9, 2015 as DOI: 10.1124/mol.115.100149
This article has not been copyedited and formatted. The final version may differ from this version.

tubulin and whether their binding modes share common features among themselves or with other structurally different vinca domain ligands remains unclear.

We determined the crystal structures of the above three agents bound to tubulin at high-resolution (≈ 2.5Å). Our data revealed that these three MTAs all bind to the vinca domain and share a common and key pharmacophore. In addition, we observed tubulysin M bound to the β subunit alone, suggesting a rationale for its higher affinity for tubulin, and our structural analysis provided a molecular mechanism for it. Finally, we found that two other representative MTAs with diverse structure targeting the vinca domain, ustiloxin D and vinblastine, shared a similar pharmacophore identified above. These findings provide the possibility for structure-based rational design of novel microtubule inhibitors targeting the vinca domain with high specificity, affinity and efficiency as payloads for ADC cancer therapy.

Molecular Pharmacology Fast Forward. Published on December 9, 2015 as DOI: 10.1124/mol.115.100149
This article has not been copyedited and formatted. The final version may differ from this version.

Materials and Methods

Porcine brain tubulin (Cat. # T-238P) was purchased from Cytoskeleton, Inc. The clone of RB3-SLD was a gift from Dr. Benoît Gigant (CNRS, France). The plasmid of TTL was also a kind gift from Dr. Michel O. Steinmetz (PSI, Switzerland). Tubulysin M and HTI-286 were purchased from Levena Biopharma Co., Ltd. MMAE was provided by Yi Qun Biotechnology Co., Ltd. Vinblastine was obtained from Selleck. Antiprotease cocktail was purchased from Sangon Biotech. Bis Tris Propane, Imidazole, Tyrosine, DTT and AMPPCP were purchased from Sigma. β-mercaptoethanol was obtained from XiYa Reagent.

Protein Expression and Purification. The stathmin-like domain of RB3 (RB3-SLD) was expressed in E.coli, purified by anion-exchange chromatography and gel filtration, concentrated to 10 mg/mL and stored at -80°C. (Charbaut et al., 2001; Dorléans et al., 2009). Protein production of TTL (tubulin tyrosine ligase) was also carried out using E.coli according to the procedure reported by Prota, et al(Prota et al., 2013a). After expression in E. coli, the protein was purified by affinity chromatography and gel filtration, concentrated to 20 mg/ml and stored at -80°C. The purity of RB3 and TTL was assessed by SDS-PAGE. Porcine brain tubulin was supplied at 10 mg/ml in G-PEM (General tubulin buffer: 80 mM PIPES pH 6.9, 2 mM $MgCl_2$, 0.5 mM EGTA and 1 mM GTP) as a frozen liquid and preserved at -80°C until use.

Protein Crystallization and Crystal Soaking. Crystals of T2-R-TTL were obtained by vapor diffusion using the sitting-drop method according to the provided protocols (Prota et al., 2013a; Prota et al., 2013b; Prota et al., 2014). The protein solution consisting of 82 µl tubulin (10 mg/ml), 9.9 µl TTL (20 mg/ml) and 8.1 µl RB3 (10mg/ml), with a molar ratio of tubulin:RB3:TTL of 2:1.3:1.2, was incubated on ice with 1 mM AMPPCP, 5 mM tyrosine and 10 mM DTT, and then concentrated to 20 mg/ml at 4°C. Crystallization drops contained 1 µl

of the T2-R-TTL protein solution and 1 μl of the precipitant solution consisting of 6% PEG4000, 5% glycerol, 0.1M MES, 30 mM $CaCl_2$, 30 mM $MgCl_2$, pH 6.7 on a sitting plate and incubated at 20°C. Crystals appeared after one day and reached a length of 200-300 μm within 3-5 days.

For crystal soaking, all ligands were dissolved in DMSO at 30 mM. MMAE (0.1 μl), tubulysin M (0.1 μl) and HTI-286 (0.1 μl) were soaked into crystals for 24h at 20°C. The crystals were transiently dipped into a cryoprotectant (30 mM $MgCl_2$, 30 mM $CaCl_2$, 0.1M MES, 20 % glycerol, pH 6.7) and flash-cooled in liquid nitrogen for Synchrotron X-ray diffraction data collection.

X-ray Data Collection, Structure Determination, Refinement and Analysis. All X-ray diffraction data were collected at beamline BL17U1 and BL19U1 at the Shanghai Synchrotron Radiation Facility (SSRF, Shanghai Institute of Applied Physics, Chinese Academy of Sciences, P. R. China) at a wavelength of 0.97915 Å and 0.97853 Å. Data were indexed, integrated and scaled using the HKL-2000 software(Otwinowski and Minor, 1997). The structure was solved by the molecular replacement method with an existing ligand-free structure T2-R-TTL (PDB code: 4I55) as our research model. The models were improved by cycles of manual rebuilding in Coot (Emsley et al., 2010) and REFMAC refinement (Vagin et al.,2004) with the CCP4 software suite (Winn et al., 2011). The final data collection and refinement statistics are summarized in Table 1. The figures are drawn using PyMol software (DeLano, 2002).

Molecular Pharmacology Fast Forward. Published on December 9, 2015 as DOI: 10.1124/mol.115.100149
This article has not been copyedited and formatted. The final version may differ from this version.

Results

Overall Structure of the Three MTAs Bound to Tubulin. Using soaked crystals of a protein complex (T2-R-TTL) consisting of α/β-tubulin, the stathmin-like protein RB3 and tubulin tyrosine ligase, we determined the structures of HTI-286, MMAE and tubulysin M (Fig. 1) bound to tubulin at 2.5-2.55Å (Table 1 and Fig. 2). The difference electron density map calculated using the ligand-omitting protein model clearly defined the envelope into which each of the three ligands could be fit unambiguously (Fig. 2B and C). The overall structure of tubulin in the three complexes superimposed well with the previously determined ligand-free structure (PDB code: 4I55), with root mean square deviation (RMSD) ranging from 0.168-0.279 Å over 700 Cα atoms, indicating little effect of the binding of each ligand on tubulin's overall structure.

HTI-286 and MMAE bind to the vinca domain, which is between tubulin subunits β1 and α2 (Fig. 2A). Surprisingly, tubulysin M bound not only to the vinca domain illustrated by TM1 but also to the tubulin β2 subunit alone illustrated by TM2 (Fig. 2A). When the β1 and β2 subunits were superimposed, the structures of TM1 and TM2 superimposed as well. The conformations of both were almost identical with the exception of small variations observed at the molecular ridges pointing away from the tubulin β subunits (Supplemental Fig. S1). These variations were due to the additional restrictions imposed on the ligand by the α2 subunit in the vinca domain. The similarity of the conformation of TM2 to TM1 indicated that the bound conformation of both is determined predominantly by the β subunit as the influence of the α subunit was absent in the structure of TM2.

Detailed Interactions of HTI-286 with Tubulin α and β Revealed the Most Important Elements for Binding to the Vinca Domain. In the vinca domain, HTI-286, MMAE and tubulysin M are sandwiched between subunits β1 and α2 and they structurally

Molecular Pharmacology Fast Forward. Published on December 9, 2015 as DOI: 10.1124/mol.115.100149
This article has not been copyedited and formatted. The final version may differ from this version.

superimposed quite well (Figs. 3 and 4). HTI-286 is the smallest ligand of the three and therefore its interactions with tubulin should display the most important elements for binding.

On the α2 subunit, HTI-286 mainly interacted with loop H7-H8, helix H10 and strand S9 (Fig 3A). Both hydrophobic and hydrogen bonding interactions were observed. Hydrophobic interactions involved the tert-butyl group (C16-C19) of HTI-286 and the hydrophobic pocket (HPα) formed mainly by Leu248 from loop H7-H8, Pro325 and Val328 from H10, and Val353 and Ile355 from S9. In addition, Ile332 from H10 and Phe351 from S9 extend HPα and contact the methyl group C21 (Fig. 3A). Two hydrogen bonding interactions with α2 were observed to be shared by the all three ligands. The first involves the side chain of Asn329 on H10 directly with O6 and N8 of HTI-286. The other is mediated by water molecules H2O-1 and H2O -3 between the main chain elements of S9 and HTI-286 (Fig. 3A).

On the β1 subunit, HTI-286 interacted with loop T5, helix H6, loop H6-H7 and helix H7 (Fig. 3B). The interactions included the following hydrophobic contacts: (1) the isopropyl side chain (C13-C15) of HTI-286 inserted into a hydrophobic pocket (HPβ) formed by Val177 from loop T5, Tyr210 from H6, and Tyr224 and Leu227 from H7; (2) the benzyl group (C24-C29) and two methyl groups (C22-C23) on the other side of the ligand contact the C-terminus of loop T5. In addition, several hydrogen bonds contributed to the binding to the β1 subunit (Fig. 3B). Asp179 from loop T5 hydrogen bonded N20 directly and also indirectly via water molecule H2O-3. Interestingly, this same N20 formed a hydrogen bond network with the main chain N and O atoms of α2 via the same H2O-3 (Fig 3A). Asp179 also hydrogen bonded O9 via water molecule H2O-1 (Fig. 3B). An additional hydrogen bond network existed between O6 of HTI-286 and the side chain of Tyr210 and the main chain of Pro222 via H2O-2.

Molecular Pharmacology Fast Forward. Published on December 9, 2015 as DOI: 10.1124/mol.115.100149
This article has not been copyedited and formatted. The final version may differ from this version.

Additional Hydrogen Bonding Interactions between MMAE and the Vinca Domain of Tubulin. The interactions between MMAE and tubulin β1 included virtually all of the components observed with HTI-286. However, because MMAE is a considerably larger molecule, there was the opportunity for additional favorable contacts such as those observed between the ligand and loop H6-H7, helix H7, loop S7-H9 and helix H1(Fig. 3D and E). The additional interactions were as follows: (1) O12 of MMAE formed a hydrogen bond with the main chain N atom from Tyr224; (2) O4 formed a hydrogen bond network with the main chain N atom from Gly225(H7), the side chains of Thr223 (H6-H7) and Arg278 (S7-H9), via water; (3) O1 formed a hydrogen bond with the side chain of Gln15 on H1.

The interactions between MMAE and the tubulin α2 subunit were quite similar to those observed for HTI-286. The hydrogen bond interactions were almost identical (Fig.3 A and C). The additional structure of MMAE (C6-C24) pointed out into the solvent and did not contribute substantially, with the exception of an extra hydrophobic contact between the pyrrolidinyl ring of MMAE and loop H7-H8 containing Ala247 and Leu248 (Fig. 3C). At the other end of MMAE (N22), the molecule did not extend as deeply into α2 as did HTI-286 where its phenyl group (C24-29) could interact with I332 (Fig. 3A vs. 3C).

Tubulysin M Bound to the Vinca Domain of Tubulin. Tubulysin M interacted with α2 in a manner almost identical to HTI-286 and MMAE (Fig. 3F). More interesting was its interaction with the β1 subunit. Like MMAE, the interaction contained almost all the components of those observed for HTI-286. The small difference was that the H-bond between Asp179 and the N19 atom, corresponding to N20 in HTI-286, was reduced due to the chiral conformation of the hexahydropyridine ring (Fig. 3G). In addition, because of its larger structure, tubulysin M formed additional interactions with loop H6-H7, helix H7, loop S7-H9 and helix H1 (Fig. 3 G and H). Similar to MMAE, the additional interactions were mainly

Molecular Pharmacology Fast Forward. Published on December 9, 2015 as DOI: 10.1124/mol.115.100149
This article has not been copyedited and formatted. The final version may differ from this version.

charged but, unlike MMAE, its structure branches allowing for different and possibly stronger interactions with subunit β1. The following interactions were observed (Fig 3 G and H): (1) N8 and O6 of tubulysin M formed hydrogen bonds with the main chain N atoms of Tyr224 and Gly225 at the N-terminus of helix H7; (2) the oxygen atoms O1a/O1b at one end of tubulysin M formed a salt bridge with the side chain of Arg278 (S7-H9); (3) an additional observation was the hydrogen bond network between tubulysin M directly with the side chain of Thr223(H6-H7) , and indirectly via H2O-3 and H2O-4 with Asn228 (H7) and Gln15 (H1). These additional interactions, especially the salt bridge, may explain why tubulysin M can bind to subunit β alone (Fig. 2A).

These Three Ligands Define a Key Fundamental Pharmacophore for Binding to the Vinca Domain of Tubulin. In summary, the bound conformations of these three peptidyl ligands shared a common and key pharmacophore, two consecutive hydrophobic groups (Val, Ile-like side chain) protruding in opposite directions into separate hydrophobic pockets on the β1 and α2 subunits of tubulin (Fig. 4A and C). Additionally, in the direction normal to the surface formed by the above hydrophobic groups, atoms N and O from the same backbone formed hydrogen bonds with Asn329 on α2 and Asp179 on β1 (Fig. 4B). These features are unique as these two consecutive amino acid residues fit snuggly into the narrowest channel between two tubulin subunits in the vinca domain and use both backbone and side chain elements to interact in all four orthogonal directions with tubulin (Fig. 4).

Two Structurally Different Vinca Domain Ligands, Ustiloxin D and Vinblastine, Share the Same Key Interacting Components. Several crystal structures of vinca domain ligands have been reported with resolutions in the range of 2.7-4.4Å (Cormier et al., 2008; Gigant et al., 2005; Ranaivoson et al., 2012). Among those, the circular molecule ustiloxin D (Fig. 1) has had its 2.7 Å structure determined when bound to tubulin that had been partially

Molecular Pharmacology Fast Forward. Published on December 9, 2015 as DOI: 10.1124/mol.115.100149
This article has not been copyedited and formatted. The final version may differ from this version.

digested with subtilisin. Superimposing tubulin β1 with bound ustiloxin D, we surprisingly found that removing the constricting group connecting C2 and C9, which circularized the molecule, revealed that the remaining portions were almost identical to the overlapping structures of the three ligands reported here (Fig. 5A-C). Specifically, an Ile-like side group at position 3 made a hydrophobic contact with HPβ and N9 made a direct hydrogen bond with the side chain of Asp179. In addition, ustiloxin D bound to α2 in two ways as well: (1) its isopropyl group at position 6 fits into HPα; (2) the amide (N7) and carboxyl (O5) of its main chain formed hydrogen bonds with O and N atoms of the side chain of Asn329, respectively (Fig. 5B).

Phomopsin A is another vinca domain ligand with its structure bound to tubulin determined at 4.1Å (Cormier et al., 2008). Due to this resolution limitation, we did not attempt to use its structure to make a superimposition. We can reasonably assume phomopsin A could adopt the same conformation as ustiloxin D because a large part of its structure is almost identical to it.

Vinblastine, a vinca domain ligand after which the domain is named, shared the least structural similarity with the compounds described above. Its structure bound to tubulin has been determined at 4.1Å (Gigant et al., 2005) and subsequently at 3.47Å (Ranaivoson et al., 2012). This structural resolution is inadequate to compare with the structural models reported here. Therefore to complete our investigation of a pharmacophore important for vinca domain binding, we determined the structure of the vinblastine complex with T2-R-TTL at 2.5Å (Table 1). Superimposing the structure we determined with the published 3.47Å structure (PDB Code: 4EB6), indicated that our structure fit the electron density envelope better (Supplement Fig. S4). Superimposing the vinblastine structure on those of the other three ligands, as was done with ustiloxin D, led to the unanticipated revelation that, despite its

Molecular Pharmacology Fast Forward. Published on December 9, 2015 as DOI: 10.1124/mol.115.100149
This article has not been copyedited and formatted. The final version may differ from this version.

structural disparity, all of the essential interactions identified with above compounds were maintained (Fig. 5D-F). Specifically, the ethyl group from the D'-ring of the catharanthine portion fit into HPβ and the N9 atom of vindoline portion formed a hydrogen bond with Asp179 (Fig. 5E). In addition, the benzyl A'-ring at the opposite side of catharanthine portion fit into the hydrophobic pocket HPα and the N atom on the B'-ring and the O atom from the side chain of the C'-ring contributed to the two hydrogen bonds with the Asn329 side chain.

Molecular Pharmacology Fast Forward. Published on December 9, 2015 as DOI: 10.1124/mol.115.100149
This article has not been copyedited and formatted. The final version may differ from this version.

Discussion

Vinca domain ligands are a class of microtubule inhibitors with great potential for cancer therapy as payloads for ADCs because of their high affinity for tubulin resulting in good clinical efficacy. Understanding the structure-activity relationships controlling tubulin binding is critical to new drug development in this area. Although several crystal structures of the complexes between MTAs and the vinca domain of tubulin have been determined, none were of sufficient resolution to serve as guides for rational drug design. As a result, no generalized consensus on a pharmacophore for ligand binding to the vinca domain of tubulin has been attained.

In the present study, the structures of four ligands bound to the vinca domain of tubulin were determined at atomic resolution (≈ 2.5Å). Of these, only the structure of the vinblastine complex had been determined previously, but only at a resolution of 3.47 Å. HTI-286, MMAE and tubulysin M compose a unique class of vinca domain ligands in that they are short peptidyl compounds. Soblidotin has a structure similar to MMAE (Fig. 2D and Supplement Fig. S2), and is the only compound in this class where a crystal structure bound to tubulin was reported (Cormier et al., 2008) but only at a resolution of 3.8 Å (PDB code: 3E22, Fig. 2D). Soblidotin differs from MMAE at 3 minor positions, which play little role in binding to tubulin (Fig. S2). While the reported orientation of soblidotin in the vinca domain was correctly defined, its precise position between the tubulin subunits is very likely incorrect. When we superimposed the tubulin β1 subunit, we found that many details of the previously determined conformation of soblidotin were different than MMAE determined at 2.5 Å. The most significant shift of about 5.5 Å occurred at the phenyl group at the tail end of the molecule (Fig. 2E). Because of this disparity, we determined that we could readily fit soblidotin into the electron density envelope of MMAE and therefore we consider the re-fitted conformation of soblidotin likely to be the correct one (Supplemental Fig. S2).

Molecular Pharmacology Fast Forward. Published on December 9, 2015 as DOI: 10.1124/mol.115.100149
This article has not been copyedited and formatted. The final version may differ from this version.

The phenomenon that tubulysin M binds not only to the vinca domain, but also to the tubulin β2 subunit alone has been observed previously for phomopsin A (Cormier et al., 2008). This suggests a rationale as to why both tubulysin M and phomopsin A have higher affinity for tubulin than HTI-286 and MMAE in that the latter two agents require interaction with both subunits for binding whereas the former do not. Thus the unrequired but additional favorable binding interactions of the former two agents with the α subunit should translate into higher affinity for the vinca site. However, an insight into the higher affinity of phomopsin A was not achieved in the previously determined crystal structure due to inadequate resolution (4.1Å). In contrast, our current study documents several additional favorable interactions observed for tubulysin M including the energetically important salt bridge with Arg278 (Fig. 3H).

By comparing the complexes for all of the structurally distinct ligands bound to the vinca domain of tubulin, we were able to define a fundamental pharmacophore for binding (Fig. 6). The pharmacophore consists of two hydrophobic regions I and II that interact with hydrophobic pockets on the β and α subunits, respectively, and two hydrogen bonding regions that interact with Asp179.β and Asn329.α. In addition to these four components, two additional regions A and B were identified where ligands can make additional favorable interactions for tighter binding. Specifically in space B, where both MMAE and tubulysin M project their additional structure, there is opportunity for structural modifications to enhance binding.

Although the conformation of phomopsin A bound to tubulin was determined only at 4.1Å (Cormier et al., 2008), it can serve as an example to illustrate our structural insights into the pharmacophore of vinca domain ligands. Its structure contains two portions—a macrocycle, which is similar to ustiloxin D and a dicarboxylate end. If only the macrocycle portion bound to the vinca domain as does ustiloxin D, its dissociation constant (Kd) should

Molecular Pharmacology Fast Forward. Published on December 9, 2015 as DOI: 10.1124/mol.115.100149
This article has not been copyedited and formatted. The final version may differ from this version.

be similar to that of ustiloxin D (1.8±0.6 μM) (Ranaivoson et al., 2012). The 10-fold higher affinity of phomopsin A (Kd <0.1 μM) (Ranaivoson et al., 2012) may be partly due to the additional dicarboxylate end that can project into space B, allowing interaction with subunit β. Interestingly, phomopsin A, like tubulysin M, bound to both the vinca domain and to the β subunit alone, while ustiloxin D, like HTI-286 and MMAE, bound only to the vinca domain. This corroborates the observation that binding to two sites in the T2-R crystal is consistent with higher affinity of the ligand for the vinca domain of tubulin.

The binding of each of the 3 vinca domain ligands causes the two tubulin subunits to bend and twist slightly as was observed previously for bound ustiloxin D (Ranaivoson et al., 2012). Aligning tubulin β1, the RMSD of the Cα atoms of the α2 subunit in the complex with bound HTI-286, MMAE and tubulysin M is 0.765, 0.863 and 2.20Å, respectively (over 440 Cα atoms). The bending and twisting of the subunits can also be visualized clearly in Supplemental Fig. S3. The larger bending caused by tubulysin M is due to the larger size of the molecule between two tubulin subunits.

In summary, we determined the structures of 4 vinca domain ligands bound to tubulin at high resolution. Three of these structures have not been reported previously and the other only at 3.47Å. Together with the high resolution structure for ustiloxin D, we analyzed their bound conformations in the vinca domain of tubulin and mapped out a common pharmacophore for the first time. We also observed that tubulysin M was able to bind to the tubulin β subunit alone and provided the structural insight into its higher affinity. This study lays a foundation for the rational design of novel MTAs with high specificity, affinity and efficiency as payloads for ADCs in cancer therapy.

Molecular Pharmacology Fast Forward. Published on December 9, 2015 as DOI: 10.1124/mol.115.100149
This article has not been copyedited and formatted. The final version may differ from this version.

Acknowledgments

We thank Dr. Benoît Gigant (CNRS, France) and Dr. Michel O. Steinmetz (PSI, Switzerland) for their kind offers of the plasmids of RB3-SLD and TTL. We thank Prof. Qiang Li (Institute of Modern Physics, Chinese Academy of sciences) and Dr. John Yun-Chung Chen (UCLA) for their kind contributions for improving this manuscript. We thank Yuqin Yao, Qinhuai Lai, Lantu Gou, Hao Chen, Qiang Chen and Dan Su for their help in the experiments and data analysis. We also acknowledge the technical expertise of Dr. Feng Yu and Dr.Wenming Qin for training us in the collection of X-ray data at the beamline BL17U1 and BL19U1 at the Shanghai Synchrotron Radiation Facility (SSRF, P. R. China).

Molecular Pharmacology Fast Forward. Published on December 9, 2015 as DOI: 10.1124/mol.115.100149
This article has not been copyedited and formatted. The final version may differ from this version.

Authorship Contributions

Participated in research design: Jinliang Yang, Rundong Zhang and Yuxi Wang

Conducted experiments: Yuxi Wang, Yangping Wu, Qisheng Wang, Yunfeng Chen, Xiangzheng Chen, Huiyan Li and Yonghui Zhang.

Performed data analysis: Rundong Zhang.

Wrote or contributed to the writing of the manuscript: Rundong Zhang, Yuxi Wang, Jinliang Yang and Frederick W. Benz.

Molecular Pharmacology Fast Forward. Published on December 9, 2015 as DOI: 10.1124/mol.115.100149
This article has not been copyedited and formatted. The final version may differ from this version.

References

Akhmanova A and Steinmetz MO (2008) Tracking the ends: a dynamic protein network controls the fate of microtubule tips. *Nat Rev Mol Cell Biol* **9**: 309-322.

Carlson K and Ocean AJ (2011) Peripheral neuropathy with microtubule-targeting agents: occurrence and management approach. *Clin Breast Cancer* **11**: 73-81.

Charbaut E, Curmi PA, Ozon S, Lachkar S, Redeker V, and Sobel A (2001) Stathmin family proteins display specific molecular and tubulin binding properties. *J Biol Chem* **276**: 16146-16154.

Cohen R, Vugts DJ, Visser GW, Stigter-van Walsum M, Bolijn M, Spiga M, Lazzari P, Shankar S, Sani M, Zanda M, and van Dongen GA (2014) Development of novel ADCs: conjugation of tubulysin analogues to trastuzumab monitored by dual radiolabeling. *Cancer Res* **74**: 5700-5710.

Cormier A, Marchand M, Ravelli RB, Knossow M, and Gigant B (2008) Structural insight into the inhibition of tubulin by vinca domain peptide ligands. *EMBO Rep* **9**: 1101-1106.

Cragg GM and Newman DJ (2004) A tale of two tumor targets: topoisomerase I and tubulin. The Wall and Wani contribution to cancer chemotherapy. *J Nat Prod* **67**: 232-244.

DeLano WL (2002) The PyMOL molecular graphics system. http://www.pymol.org.

Dorléans A, Gigant B, Ravelli RB, Mailliet P, Mikol V, and Knossow M (2009) Variations in the colchicine-binding domain provide insight into the structural switch of tubulin. *Proc Natl Acad Sci U S A* **106**: 13775-13779.

Dumontet C and Jordan MA (2010) Microtubule-binding agents: a dynamic field of cancer therapeutics. *Nat Rev Drug Discov* **9**: 790-803.

Emsley P, Lohkamp B, Scott WG, and Cowtan K (2010) Features and development of Coot. *Acta Crystallogr D Biol Crystallogr* **66**: 486-501.

Etienne-Manneville S (2010) From signaling pathways to microtubule dynamics: the key players. *Curr Opin Cell Biol* **22**: 104-111.

Etienne-Manneville S and Hall A (2002) Rho GTPases in cell biology. *Nature* **420**: 629-635.

Gigant B, Wang C, Ravelli RB, Roussi F, Steinmetz MO, Curmi PA, Sobel A, and Knossow M (2005) Structural basis for the regulation of tubulin by vinblastine. *Nature* **435**: 519-522.

Hartley RM, Peng J, Fest GA, Dakshanamurthy S, Frantz DE, Brown ML, and Mooberry SL (2012) Polygamain, a new microtubule depolymerizing agent that occupies a unique pharmacophore in the colchicine site. *Mol Pharmacol* **81**: 431-439.

Klute K, Nackos E, Tasaki S, Nguyen DP, Bander NH and Tagawa ST (2014) Microtubule inhibitor-based antibody–drug conjugates for cancer therapy. *Onco Targets Ther* **7**: 2227-2236.

Komlodi-Pasztor E, Sackett DL, and Fojo AT (2012) Inhibitors targeting mitosis: tales of how great drugs against a promising target were brought down by a flawed rationale. *Clin Cancer Res* **18**: 51-63.

Muldoon LL, Soussain C, Jahnke K, Johanson C, Siegal T, Smith QR, Hall WA, Hynynen K, Senter PD, and Peereboom DM (2007) Chemotherapy delivery issues in central nervous system malignancy: a reality check. *J Clin Oncol* **25**: 2295-2305.

Otwinowski Z and Minor W (1997) Processing of X-ray diffraction data collected in oscillation mode. *Macromol Crystallogr A* **276**: 307–326

Poruchynsky MS, Kim JH, Nogales E, Annable T, Loganzo F, Greenberger LM, Sackett DL, and Fojo T (2004) Tumor cells resistant to a microtubule-depolymerizing hemiasterlin analogue, HTI-286, have mutations in alpha- or beta-tubulin and increased microtubule stability. *Biochemistry* **43**: 13944-13954.

Prota AE, Bargsten K, Northcote PT, Marsh M, Altmann KH, Miller JH, Diaz JF, and Steinmetz MO (2014) Structural basis of microtubule stabilization by laulimalide and peloruside A. *Angew Chem Int Ed Engl* **53**: 1621-1625.

Prota AE, Bargsten K, Zurwerra D, Field JJ, Díaz JF, Altmann KH, and Steinmetz MO (2013a) Molecular mechanism of action of microtubule-stabilizing anticancer agents. *Science* **339**: 587-590.

Prota AE, Magiera MM, Kuijpers M, Bargsten K, Frey D, Wieser M, Jaussi R, Hoogenraad CC, Kammerer RA, Janke C, and Steinmetz MO (2013b) Structural basis of tubulin tyrosination by tubulin tyrosine ligase. *J Cell Biol* **200**: 259-270.

Ranaivoson FM, Gigant B, Berritt S, Joullié M, and Knossow M (2012) Structural plasticity of tubulin assembly probed by vinca-domain ligands. *Acta Crystallogr D Biol Crystallogr* **68**: 927-934.

Ravelli RB, Gigant B, Curmi PA, Jourdain I, Lachkar S, Sobel A, and Knossow M (2004) Insight into tubulin regulation from a complex with colchicine and a stathmin-like domain. *Nature* **428**: 198-202.

Risinger AL, Giles FJ, and Mooberry SL (2009) Microtubule dynamics as a target in oncology. Cancer Treat Rev **35**: 255-261.

Roque DM, Bellone S, English DP, Buza N, Cocco E, Gasparrini S, Bortolomai I, Ratner E, Silasi DA, and Azodi M (2013) Tubulin-β-III overexpression by uterine serous carcinomas is a marker for poor overall survival after platinum/taxane chemotherapy and sensitivity to epothilones. *Cancer* **119**: 2582-2592.

Vagin A, Steiner R, Lebedev A, Potterton L, McNicholas S, and Long FM (2004) REFMAC5 dictionary: organization of prior chemical knowledge and guidelines for its use. *Acta Crystallogr D Biol Crystallogr* **60**: 2184-95.

Winn MD, Ballard CC, Cowtan KD, Dodson EJ, Emsley P, Evans PR, Keegan RM, Krissinel EB, Leslie AG, and McCoy A (2011) Overview of the CCP4 suite and current developments. *Acta Crystallogr D Biol Crystallogr* **67**: 235-242.

Molecular Pharmacology Fast Forward. Published on December 9, 2015 as DOI: 10.1124/mol.115.100149
This article has not been copyedited and formatted. The final version may differ from this version.

Footnotes

Work in the authors' laboratory was supported by research funding from the National Major Scientific and Technological Special Project for "Significant New Drug Development" [2012ZX09103301-030] and National Natural Science Foundation of China [81372822].

Molecular Pharmacology Fast Forward. Published on December 9, 2015 as DOI: 10.1124/mol.115.100149
This article has not been copyedited and formatted. The final version may differ from this version.

Figure legends

Figure 1. Chemical structures of the compounds in this study.

Figure 2. Overview of a T2-R-TTL-ligand complex structure and the conformations of the bound ligands. A. Overview of the T2-R-TTL-tubulysin M complex. Tubulin (gray), RB3 (sage green), and TTL (pale green) are depicted in ribbon representation; Tubulysin M (TM1 or TM2, orange), GDP (green) and GTP (red) are shown in spheres representation. **B.** Omit maps of the four ligands (Contoured at 3σ): HTI-286 (blue), MMAE (green), TM1 (orange) and TM2 (pink) are shown in sticks representation. **C.** The conformation of MMAE inside the electron density omit map determined at 2.55Å against tubulin β subunit. **D.** The conformation of soblidotin, which is very similar to MMAE in structure, inside the electron density omit map determined at 3.8Å against tubulin β subunit (PDB code: 3E22). **E.** Comparison of the conformations of MMAE and soblidotin with superimposition of tubulin β subunit. The curved double-ended arrows indicate the distance difference in Å of the corresponding atoms.

Figure 3. Detailed interactions of HTI-286, MMAE and tubulysin M with the tubulin vinca domain. HTI-286 interaction with the α2-domain **(A)** and β1-domain **(B)**. MMAE interaction with the α2-domain **(C)** and β1-domain **(D-E)**. Tubulysin M interaction with the α2-domain **(F)** and β1-domain **(G-H)**. See text for details.

Figure 4. Comparison of the interactions of HTI-286, MMAE and tubulysin M with tubulin. When the structures of the three ligands bound to subunit β1 are superimposed, the three structures largely overlap. Two Val- or Ile-like hydrophobic side chains protrude from consecutive positions of the ligand backbones and fit into hydrophobic pockets α and β, as seen in **(A)** and **(C)**. Three hydrogen bond interactions with either D179.β1 or N329.α2 were observed as depicted in **(B)**. These hydrophobic and hydrogen bond interactions were found

Molecular Pharmacology Fast Forward. Published on December 9, 2015 as DOI: 10.1124/mol.115.100149
This article has not been copyedited and formatted. The final version may differ from this version.

to be common to all ligands. MTAs are shown in stick representation and colored as in Fig. 2. Tubulin α2 and β1 are shown in surface representation.

Figure 5. Comparison of the structures of ustiloxin D and vinblastine with HTI-286, MMAE and tubulysin M in their tubulin-bound conformations. The ligand-bound tubulin β1s are superimposed and the conformations of bound ligands are compared. The three ligands, HTI-286, MMAE and tubulysin M are in the same orientation as in Fig. 3 but shown in line representation. The tubulin-bound conformation of ustiloxin D **(A-C)**. The tubulin-bound conformation of vinblastine (PDB code: 5BMV) **(D-F)**. Interestingly, both ustiloxin D and vinblastine contain the same common functional elements identified in Fig. 3 and summarized in Fig. 4.

Figure 6. Pharmacophore of vinca domain ligands. The pharmacophore contains two hydrophobic groups (large spheres I and II), and three hydrogen-bond-forming atoms (small spheres, blue for N atom, red for O atom). The two hydrophobic groups I and II interact with hydrophobic pockets β and α respectively. The small grey spheres represent C atoms at the edges of the hydrophobic groups. The three hydrogen-bond-forming atoms interact with D179.β (one N atom) and N329.α (one N and one O atom). There are two areas (A and B) at the opposite sides of the pharmacophore where extra chemical groups can be added to make additional interactions to increase the affinity of the ligand.

Molecular Pharmacology Fast Forward. Published on December 9, 2015 as DOI: 10.1124/mol.115.100149
This article has not been copyedited and formatted. The final version may differ from this version.

Table 1. Data collection and refinement statistics

Ligand **PDB ID code**	**HTI-286** 4ZI7	**MMAE** 4ZHQ	**Tubulysin M** 4ZOL	**Vinblastine** 5BMV
Data collection statistics				
X-ray source	SSRF-BL17U1	SSRF-BL17U1	SSRF-BL17U1	SSRF-BL19U1
Wavelength (Å)	0.97915	0.97915	0.97915	0.97853
Resolution range (Å)[a]	50.0-2.50 (2.54-2.50)	39.34-2.55 (2.59-2.55)	50.0-2.50 (2.54-2.50)	50.0-2.50 (2.54-2.50)
Space group	$P2_12_12_1$	$P2_12_12_1$	$P2_12_12_1$	$P2_12_12_1$
Unit cell: Ambic (Å)	105.31, 157.26, 181.78	104.94, 156.81, 182.47	105.13,154.82, 186.52	105.47, 157.43, 183.19
Total reflections	734243	723140	771643	709659
Unique reflections	103939 (5093)	98202 (4843)	105685 (5207)	106106 (5233)
Redundancy	7.1 (6.6)	7.4 (7.3)	7.3 (7.3)	6.7 (6.8)
Completeness (%)	99.8 (99.4)	99.9 (100)	99.9 (100)	100 (100)
Mean I/sigma (I)	14.1 (2.0)	13.7 (2.1)	18.6 (2.53)	19.0 (2.75)
Remerge	0.179 (0.90)	0.129 (0.93)	0.137 (0.884)	0.105 (0.776)
Refinement statistics				
R-factor/ R-free	0.184/0.239	0.185/0.2444	0.173/0.231	0.184/0.235
RMSD bond length (Å)	0.0146	0.0134	0.0152	0.0138
RMSD bond angle (°)	1.7415	1.6928	1.9217	1.727
Ramachandran plot statistics				
Favored regions (%)	95.6	95.3	95.1	95.2
Additional allowed regions (%)	3.9	4.2	4.3	4.3
Disallowed regions (%)	0.5	0.5	0.6	0.5

[a] The highest resolution shell is shown in parenthesis.

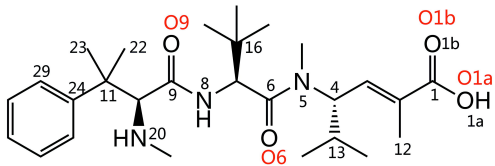

HTI-286

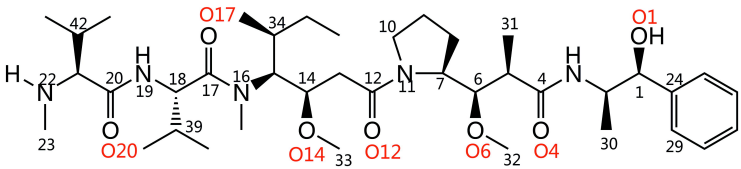

MMAE

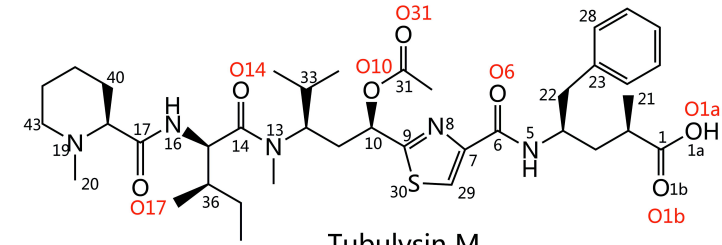

Tubulysin M

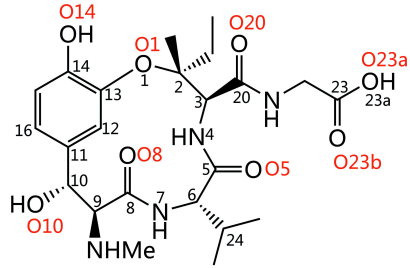

Ustiloxin D

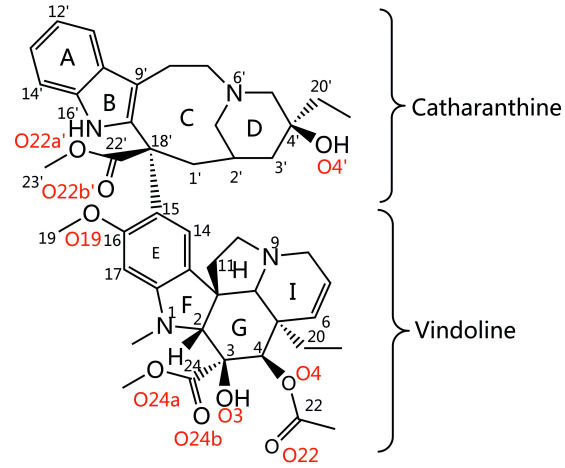

Vinblastine

Figure 1

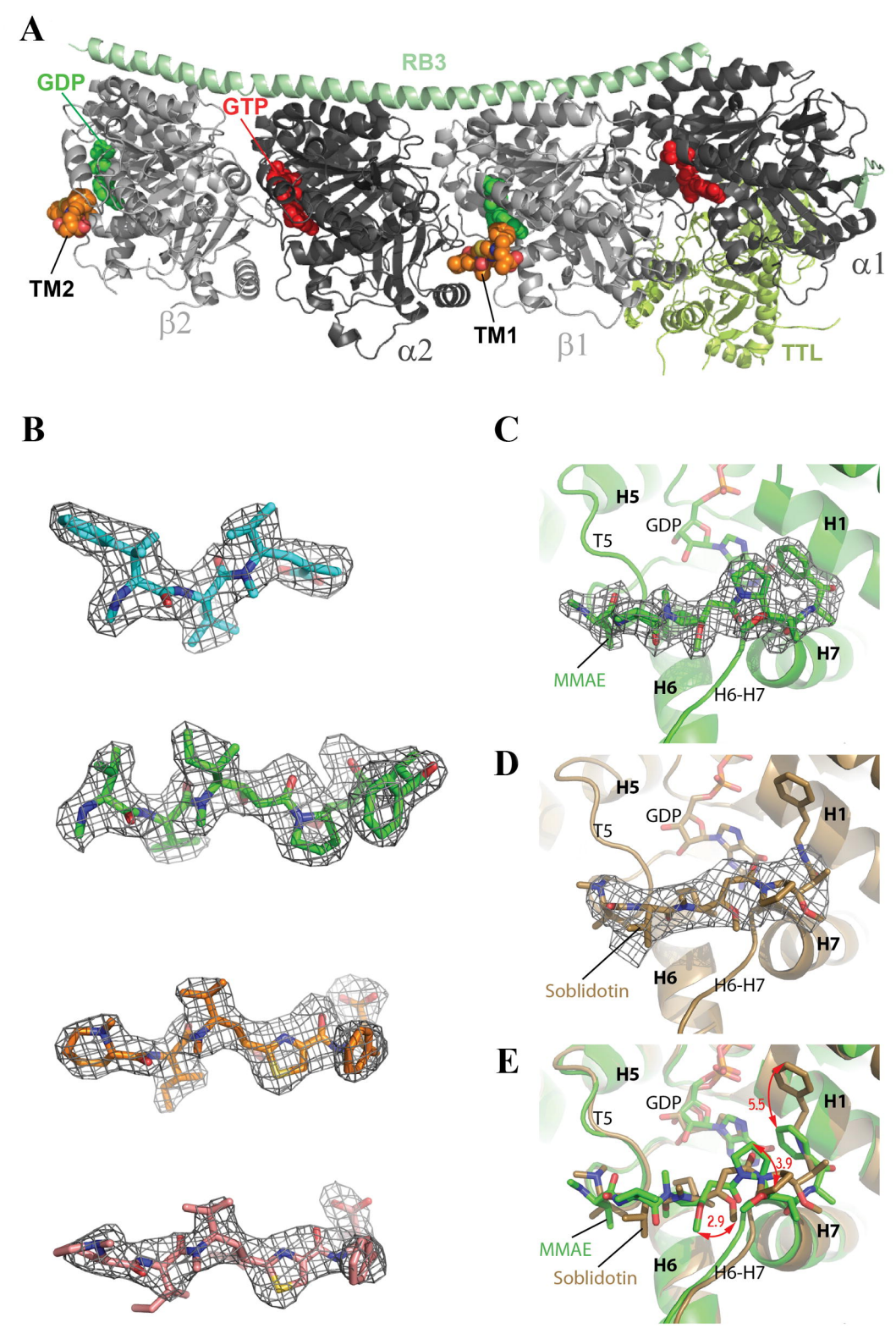
A
RB3
GDP
GTP
TM2
β2
α2
TM1
β1
α1
TTL
B
C
H5
T5
GDP
H1
H7
MMAE
H6
H6-H7
D
H5
T5
GDP
H1
H7
Soblidotin
H6
H6-H7
E
H5
T5
GDP
5.5
H1
3.9
2.9
H7
MMAE
Soblidotin
H6
H6-H7

Figure 2

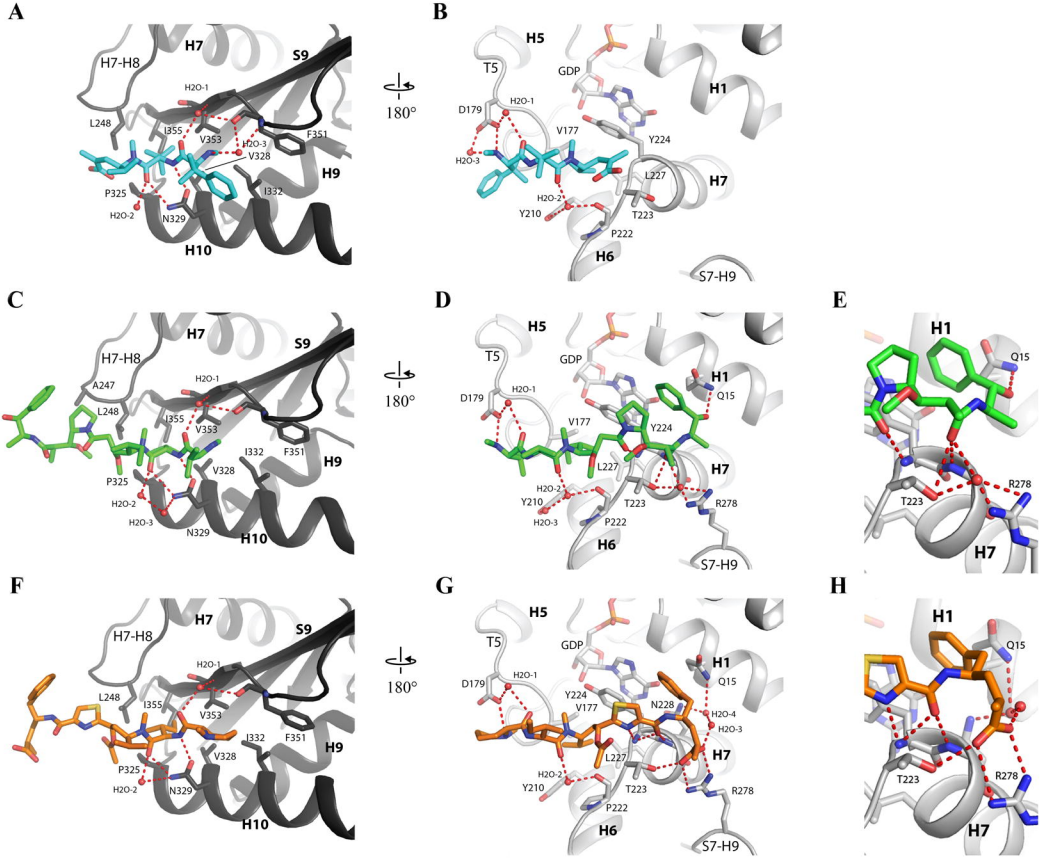
A
H7
S9
H7-H8
H2O-1
L248
I355
V353
H2O-3
V328
F351
H9
P325
H2O-2
N329
I332
H10
180°
B
H5
T5
GDP
H1
D179
H2O-1
V177
Y224
H2O-3
L227
H7
H2O-2
Y210
T223
P222
H6
S7-H9
C
H7
S9
H7-H8
A247
H2O-1
L248
I355
V353
I332
F351
H9
P325
V328
H2O-2
H2O-3
N329
H10
180°
D
H5
T5
GDP
H1
Q15
D179
H2O-1
V177
Y224
L227
H7
H2O-2
Y210
T223
R278
H2O-3
P222
H6
S7-H9
E
H1
Q15
R278
T223
H7
F
H7
S9
H7-H8
H2O-1
L248
I355
V353
I332
F351
H9
P325
V328
H2O-2
N329
H10
180°
G
H5
T5
GDP
H1
Q15
D179
H2O-1
Y224
V177
N228
H2O-4
H2O-3
L227
H7
H2O-2
Y210
T223
R278
P222
H6
S7-H9
H
H1
Q15
R278
T223
H7

Figure 3

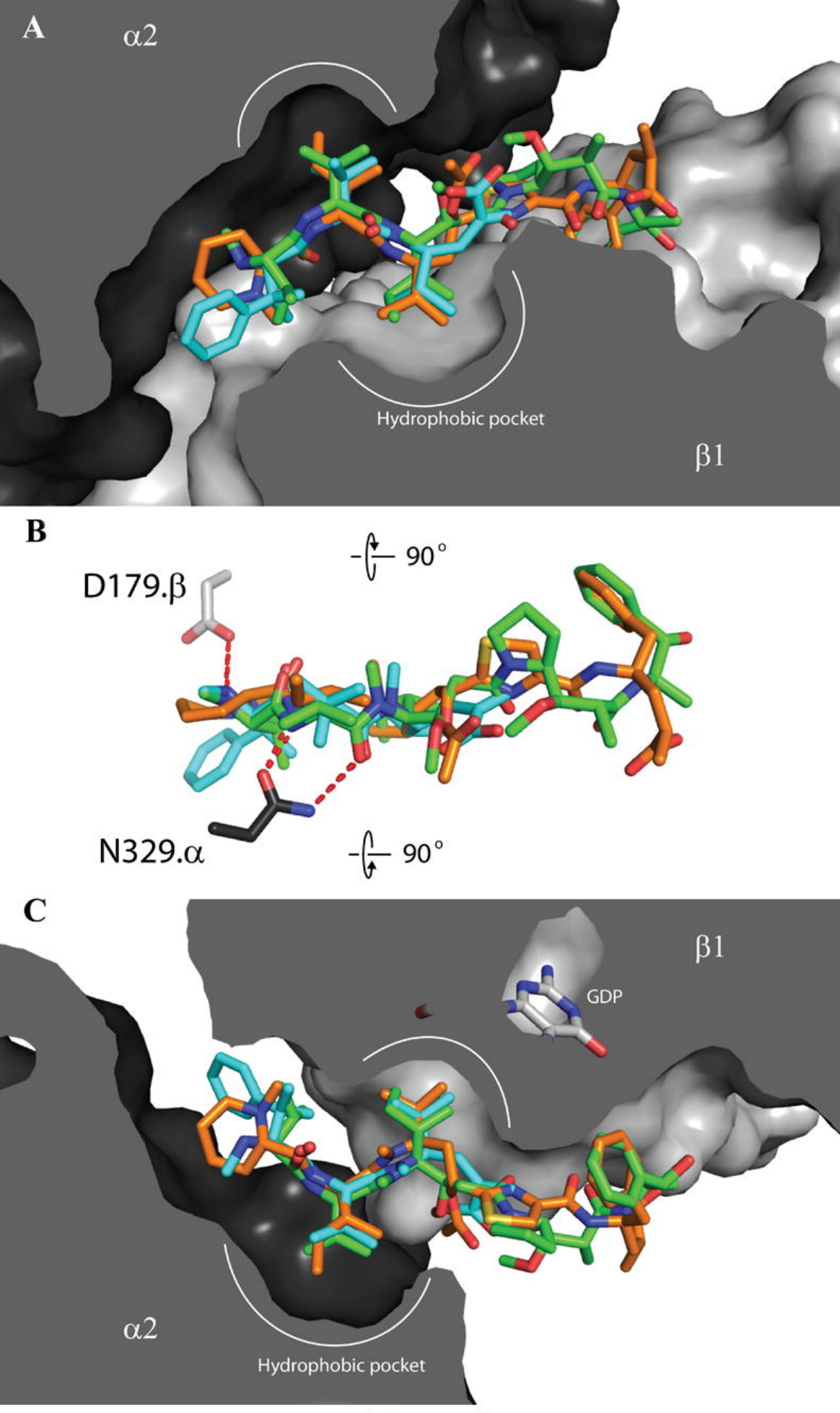
A
α2
Hydrophobic pocket
β1
B
90°
D179.β
N329.α
90°
C
β1
GDP
α2
Hydrophobic pocket

Figure 4

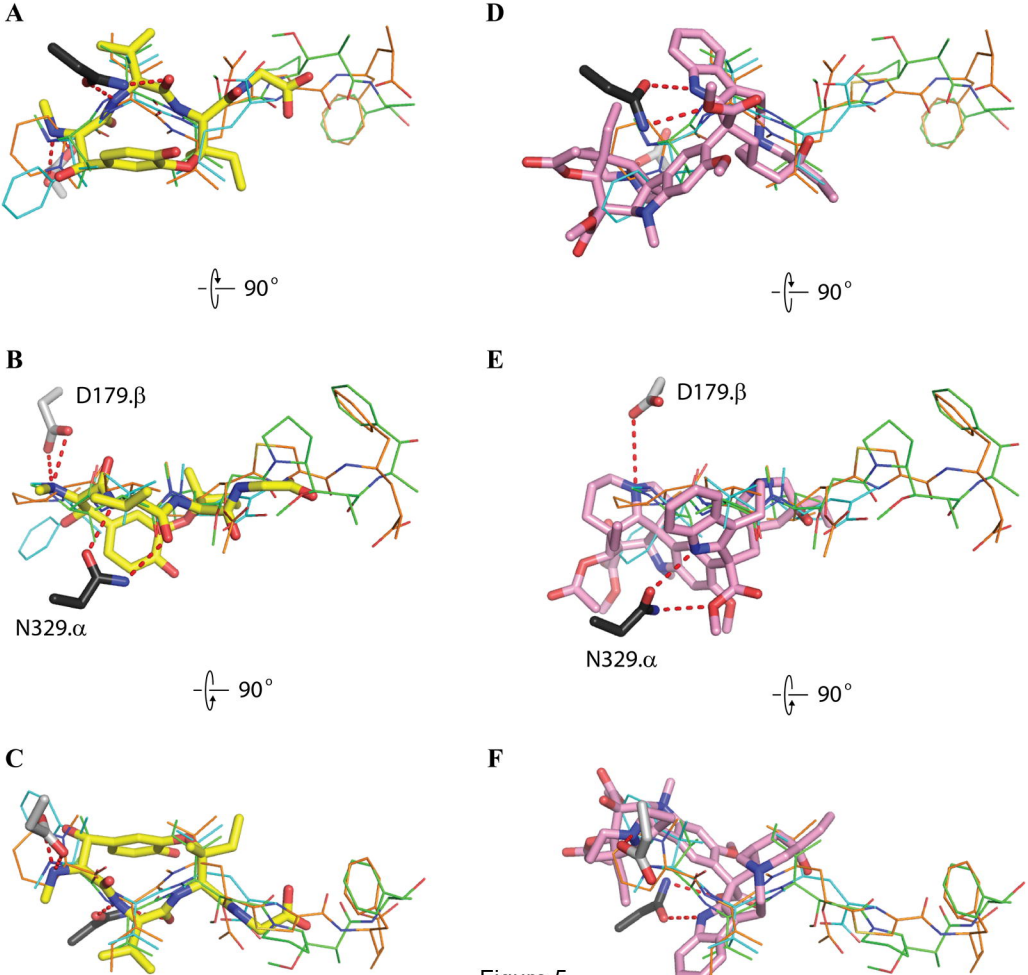

Figure 5

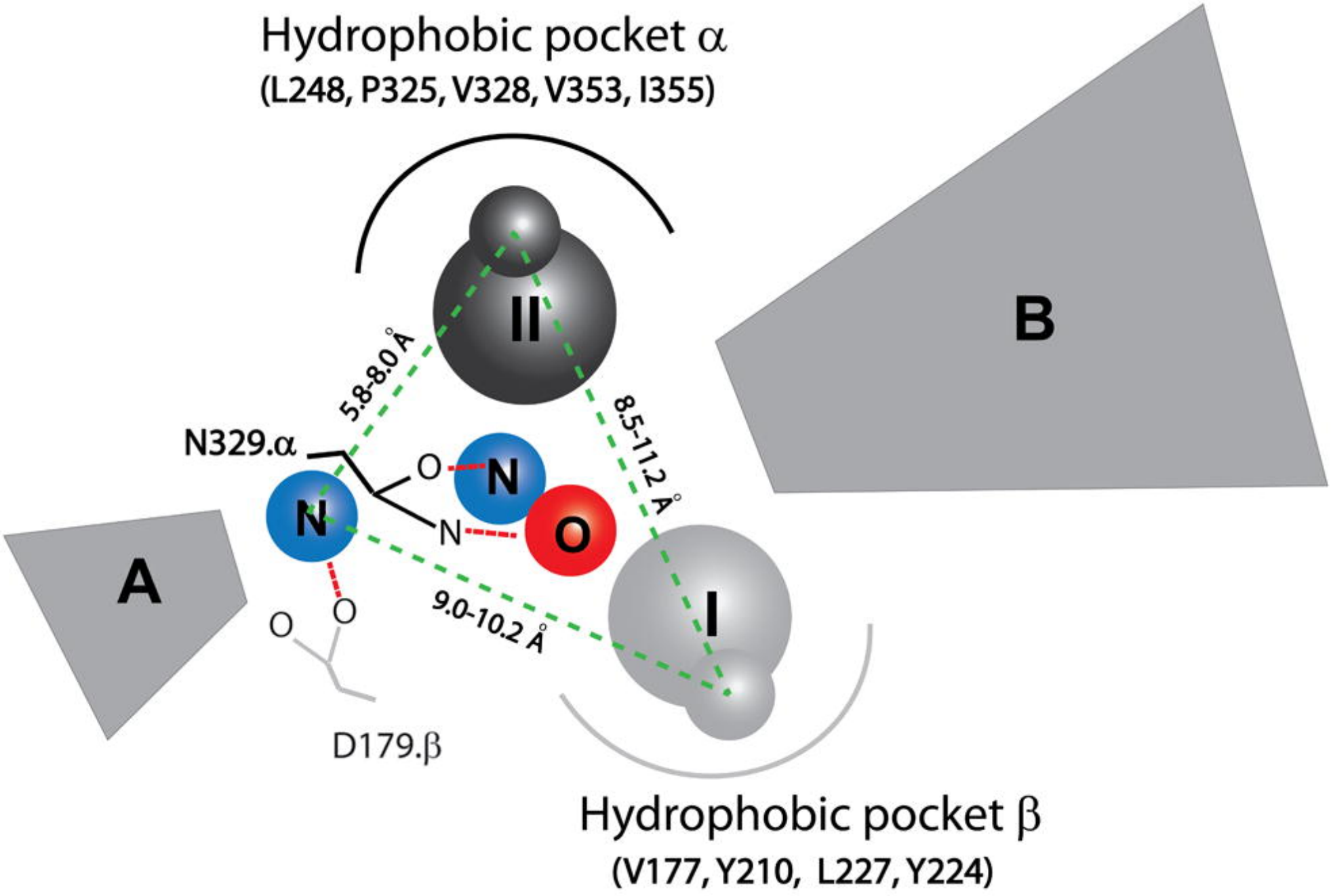
Hydrophobic pocket α
(L248, P325, V328, V353, I355)
II
B
5.8-8.0 Å
8.5-11.2 Å
N329.α
O
N
N
O
A
O
O
9.0-10.2 Å
I
D179.β
Hydrophobic pocket β
(V177, Y210, L227, Y224)

Figure 6